Acta Oceanol. Sin., 2020, Vol. 39, No. 9, P. 18–24
https://doi.org/10.1007/s13131-020-1644-7
http://www.hyxb.org.cn
E-mail: hyxbe@263.net

Comparison of summer Arctic sea ice surface temperatures from *in situ* and MODIS measurements

Na Li[1, 2*], Bingrui Li[1, 2], Ruibo Lei[1, 2], Qun Li[1, 2]

[1] Polar Research Institute of China, Shanghai 200136, China

[2] MNR Key Laboratory for Polar Science, Polar Research Institute of China, Shanghai 200136, China

Received 26 October 2019; accepted 18 November 2019

Abstract

Ship-borne infrared radiometric measurements conducted during the Chinese National Arctic Research Expedition (CHINARE) in 2008, 2010, 2012, 2014, 2016 and 2017 were used for in situ validation studies of the Moderate Resolution Imaging Spectroradiometer (MODIS) sea ice surface temperature (IST) product. Observations of sea ice were made using a KT19.85 radiometer mounted on the Chinese icebreaker *Xuelong* between July and September over six years. The MODIS-derived ISTs from the satellites, Terra and Aqua, both show close correspondence with ISTs derived from radiometer spot measurements averaged over areas of 4 km× 4 km, spanning the temperature range of 262–280 K with a ±1.7 K (Aqua) and ±1.6 K (Terra) variation. The consistency of the results over each year indicates that MODIS provides a suitable platform for remotely deriving surface temperature data when the sky is clear. Investigation into factors that cause the MODIS IST bias (defined as the difference between MODIS and KT19.85 ISTs) shows that large positive bias is caused by increased coverage of leads and melt ponds, while large negative bias mostly arises from undetected clouds. Thin vapor fog forming over Arctic sea ice may explain the cold bias when cloud cover is below 20%.

Key words: sea ice surface temperature, thermal radiometer, MODIS, Arctic Ocean

Citation: Li Na, Li Bingrui, Lei Ruibo, Li Qun. 2020. Comparison of summer Arctic sea ice surface temperatures from *in situ* and MODIS measurements. Acta Oceanologica Sinica, 39(9): 18–24, doi: 10.1007/s13131-020-1644-7

1 Introduction

Recently, much attention has been paid to the rapid decline of Arctic sea ice. Observations show a fundamental shift in the character of the Arctic sea ice cover from multiyear ice to seasonal ice, a constant shrink of ice thickness and a lengthening of the summer melt season (Comiso, 2012; Laxon et al., 2013; Markus et al., 2009). Ice surface temperature (IST), which is a crucial variable of the Arctic climate, can indicate the presence of surface melt on summer sea ice and can be considered as an integrator of surface energy fluxes. Accurate and consistent measurements of IST are needed to improve the estimation of the surface heat fluxes and our understanding and ability to predict the effects of climate change in the Arctic.

Because of the logistical obstacles in establishing a suitably dense observing network for *in situ* IST measurements in the Arctic, satellite sensors have been an important source of basin-wide information with their extensive and continual coverage. IST can be mapped globally using the infrared (IR) sensors under clear-sky conditions. The primary instruments for which such IR data have been available are the Advanced Very High Resolution Radiometer (AVHRR) and the Moderate Resolution Imaging Spectroradiometer (MODIS). The accuracy of these IR-derived IST products is affected by clouds and uncertainties regarding the radiative properties of sea ice surface. Superseding the more-limited capability of AVHRR, MODIS provides additional spectral information that is particularly useful for polar cloud detection and has water vapor bands and carbon dioxide bands that peak low in the troposphere (Hall et al., 2004). In the present paper, MODIS IST products were used for the comparison study.

Comparisons between ISTs from satellite data and *in situ* measurements have been carried out repeatedly in the Arctic. *In situ* measurements during the field campaign of Surface Heat Budget of the Arctic (SHEBA) and other field experiments show that the clear-sky AVHRR-derived IST can be estimated with an accuracy of 0.3–3.0 K (Lindsay and Rothrock, 1994; Yu et al., 1995; Haggerty et al., 2003). Key et al. (1997) attributed the larger errors of AVHRR-derived IST to spatial heterogeneity of the surface. With Comparison of the near-surface air temperatures obtained from tide stations and from drifting buoys in the Arctic Ocean, the 1-km resolution MODIS IST product shows a bias (mean error) of –2.1 K and a root mean square (RMS) error of 3.7 K (Hall et al., 2004). These validation activities were conducted mostly during the cold period (when melt water is generally not present) and uncertainties would be reduced if the skin temperature of the surface were used instead of the near-surface air temperatures.

An infrared radiometer on board the R/V *Xuelong* was used to measure skin temperature during the Chinese National Arctic Research Expedition (CHINARE) cruises that conducted in summer-fall season (warm period). This provides an additional assessment of the uncertainties in these satellite IR-derived IST products. To examine the reliability of such derivations sufficiently, the field experiments of CHINARE-2008, CHINARE-2010, CHINARE-2012, CHINARE-2014, CHINARE-2016 and CHINARE-

Foundation item: The National Natural Science Foundation of China under contract No. 41606222; the National Key Research and Development Project under contract No. 2016YFC1400303.
*Corresponding author, E-mail: lina@pric.org.cn

2017 were used in the present study.

2 CHINARE cruises and study area

Since 2008, the CHINARE cruises have taken place between July and September about every two years. From the tracks of *Xuelong* (Fig. 1), we can find that the cruises were mostly located in the Pacific Arctic Ocean, where the most significant decline of summer Arctic sea ice extent has occurred (Lei et al., 2012; Xia et al., 2014). Most of the tracks were also along the marginal ice zone (MIZ), which was the site of strong ocean-atmosphere interactions and usually visited by intense storm activities known as polar lows, and cold-air outbreak (Comiso, 2010). The central Arctic Ocean and the Arctic shipping routes, the Northeast Passage in 2012 and the Northwest Passage in 2017, are also covered.

A set of equipment were used for sea ice observations along the CHINARE cruises (Fig. 2), from which ice surface temperature, sea ice thickness and sea ice surface characteristics could be obtained.

3 Datasets and methods

3.1 *In situ measurements*

The thermal radiometer used in this work was a Helitronics KT19.85 pyrometer, which can detect radiation within the spectral range of 9.6–11.5 μm over a field of view (FOV) of 2°. It operated over a temperature range from –20°C to 70°C and was mounted on the top of the port side rail (Fig. 2). The radiometer was set in a protective jacket and not temperature controlled for summer cruises. Brightness temperature variations caused by different viewing angle were just several tenths of a Kelvin. To minimize effects of ship splash and fresh fractures created while underway, a viewing angle of 30° was selected, giving a target spot diameter of 0.5 m (Scambos et al., 2006).

KT19.85 brightness temperatures can be converted to corresponding skin temperature with the emissivity corrections (Kearns et al., 2000; Scambos et al., 2006). In the sensitivity range of KT19.85 (9.6–11.5 μm), the mean ice emissivity is high at all incidence angles, and would be 0.998 under nadir-viewing conditions (Dozier and Warren, 1982). Therefore, we applied a mean

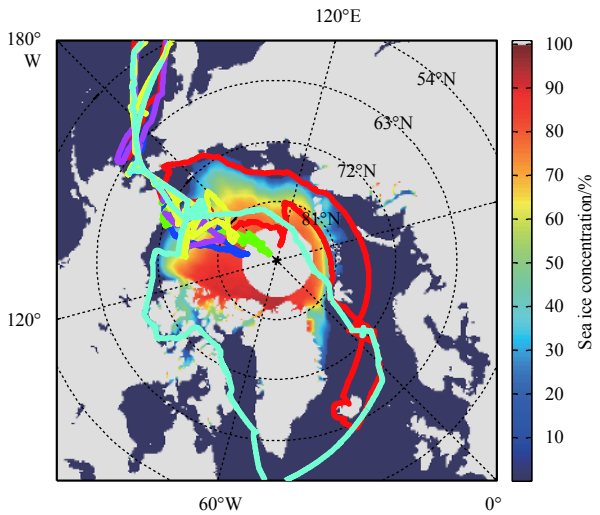

Fig. 1. Trajectories of *Xuelong* during CHINARE in 2008 (blue line), 2010 (green line), 2012 (red line), 2014 (magenta line), 2016 (yellow line), and 2017 (cyan line), colored with climatological average of September sea ice concentration for 1979–2017.

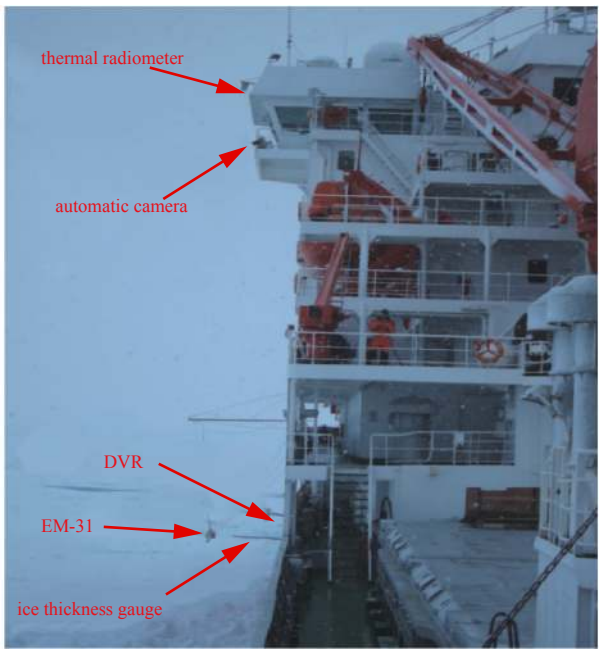

Fig. 2. Set of equipment for sea ice observations, with the KT19.85 thermal radiometer on the top.

spectral emissivity value of 1.0 and no emissivity correction. Absolute accuracy of the sensors is ±0.5°C plus 0.7% of the difference between the sensor housing temperature and scene temperature.

Following the improved Antarctic Sea Ice Processes & Climate (ASPeCt) protocol, surface characteristics of sea ice and meteorological variables were observed synchronously during the CHINARE cruises. Through the bridge-based observations, data were recorded every half an hour within a field of view (FOV) of 2 km. A full description of the ASPeCt data quality control and processing can be found in Worby et al. (2008).

3.2 *Satellite observations*

The MODIS is onboard both the Earth Observing System (EOS) satellites, Terra and Aqua. IST can be mapped from MODIS as a sequence of products. The swath-based product has a nominal swath coverage of 2 330 km×2 030 km and covers about 5 min of satellite travel. Automated selection of the most favorable observation (daytime observations that are near nadir, acquired near noon local time, and cover a large area in a grid cell) from all the swaths acquired during a day generates a daily gridded sea ice product. A daily global product of IST can be developed at 4 km resolution, also eight-day composite and monthly sea ice products are available. Detailed information on the MODIS IST products may be found in Hall et al. (2004). Because the swath algorithm will often map clouds as sea ice, we have chosen the Collection6 (C6) 4 km resolution daily global Level 3 daytime IST standard products, MOD29E1D (Terra) and MYD29E1D (Aqua) in our study. Revisions and improvements in C6 products include MODIS Level 1B calibration, the MODIS land and water mask, and the cloud mask. In science tests with C6 inputs, ±0.1 K differences of IST were found compared to the tests made with C5 inputs across all conditions (Riggs and Hall, 2015).

In an ideal comparison, the satellite and *in situ* observations would be simultaneous and precisely collocated. Several factors

should be considered in the selection of data for comparison, including sub-grid cell spatial variability of the surface (ice, leads and melt ponds), the variation of temperature over time (diurnal variation etc.) (Scambos et al., 2006). In summer, considering the persistent cloud cover and the relatively uniform surface temperature near the freezing point, here we accepted the 3-h time difference as nearly simultaneous (Yu et al., 1995). The KT19.85 measurements close to the acquisition time of MODIS IST data (±3 h) are selected. All the selected KT19.85 measurements collected within 2 km of the satellite grid cell's center were averaged and then compared with the corresponding MODIS IST estimates.

To assess the influence of different parameters to the uncertainties of MODIS IST products, a number of environmental variables are used in this study. Sea ice concentration with a spatial resolution of 6.25 km was obtained from the daily Advanced Microwave Scanning Radiometer (AMSR2 and AMSR-E) sea ice maps developed by University of Bremen. The four-times daily air temperature at 2 m, wind at 10 m, surface air pressure and daily mean cloud fraction are extracted from National Centers for Environmental Prediction-Department of Energy (NCEP-DOE) Reanalysis 2 data.

4 Results

4.1 *Sea/ice surface temperature from KT19.85 measurements*

Figure 3 showed the sea/ice surface temperature measured along *Xuelong*'s track by the KT19.85 during six CHINARE cruises. Mostly around the melting point, the measured ice/sea surface temperature ranged from 268 K to 278 K. For the northbound leg, the sea/ice surface temperature gradually decreases as *Xuelong* travels into the ice-covered and high-latitude ocean; while for the southbound leg, although it has been close to the end of melting season, the surface of the ocean was still in a state of thermal saturation and the sea/ice surface temperature gradually increases. Significant temporal and spatial variability of surface temperature also can be found in Fig. 3, which will not be specifically described in this study.

4.2 *Comparison of MODIS and KT19.85 ISTs*

Table 1 provides an overall assessment of the uncertainty of the MODIS-derived ISTs relative to the KT19.85 surface skin temperatures. As shown in Table 1, there are some outliers differ significantly (>10 K) from the full dataset. To better resolve the expected cold bias in the IST values, a filter, which could dramatically reduce the cloud affected and other anomalous IST values, was used to reduce the overall variability in the dataset. Radionov et al. (1997) and Minnett (2003) showed that the average ice/snow temperature was 0.8 K lower than the 2 m air temperature (T_{air}) in the Arctic Basin during the warm period (defined as June through August). Under cloud-free conditions, the difference could reach 6–7 K because of longwave radiative cooling. Based on these studies and following Shuman et al. (2014), a MODIS IST-T_{air} ±5 K filter was applied on the MODIS IST products. The filtering reduces the mean Aqua MODIS IST bias by 1.1 K and Terra MODIS IST bias by 0.6 K. It reduces the overall variability in the dataset, while ensuring the majority of the data available for the additional steps in the analysis without unevenly influencing any part of the overall data range (Shuman et al., 2014). The number of data points in the filtered dataset is

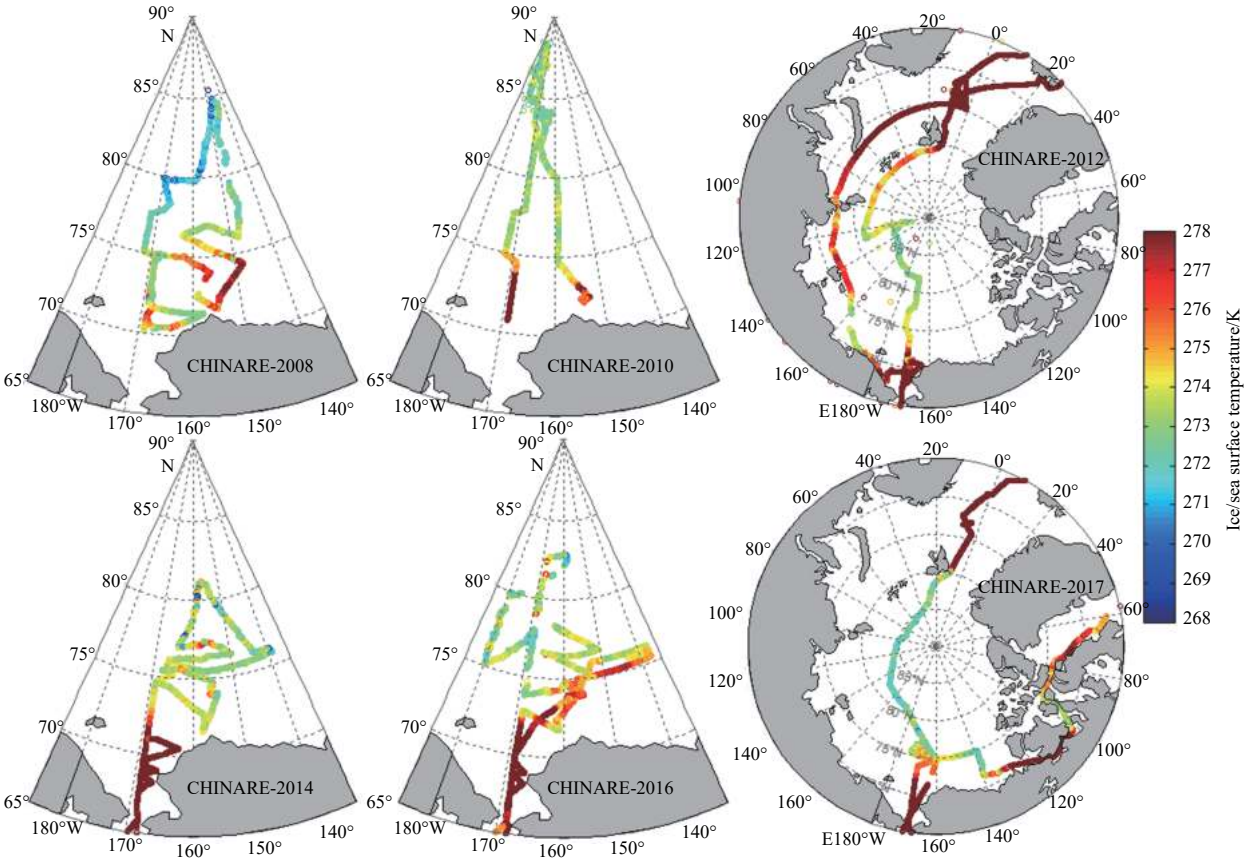

Fig. 3. Surface temperature of sea ice or open water along *Xuelong*'s track measured by KT19.85 during CHINARE cruises.

Table 1. Summary statics for the MODIS IST bias (defined as the difference between MODIS and KT19.85 ISTs) for overall data

	Number of points	Min/K	Max/K	Mean/K	Std dev/K	RMS/K
Aqua (all)	587	–24.8	5.1	–2.7	3.8	14.9
Aqua (filt.)	534	–7.8	5.1	–1.6	1.7	2.9
Terra (all)	1 046	–21.4	4.9	–2.8	3.0	8.9
Terra (filt.)	973	–9.5	4.9	–2.2	1.6	2.6

Note: "all" and "filt." indicate that the data were examined before and after applying a filter. See text for the rationale for applying the filter.

above 90% that of the original dataset and the filtered dataset is used for the rest of the study.

A total of 534 samples from Aqua and 973 samples from Terra were obtained from the comparison of all the six CHINARE cruises (Table 1). The mean MODIS IST bias is –1.6 K (for Aqua samples and –2.2 K for Terra samples) with a standard deviation of 1.7 K (for Aqua samples and 1.6 K for Terra samples), giving a RMS difference of 2.9 K (for Aqua samples and 2.6 K for Terra samples). The negative bias, which also can be obviously seen in the scatter plot in Fig. 4, indicates that MODIS is consistently underestimating IST. This cold bias is common for the IR sensors, which at least in part, may be caused by inadequacies in the atmospheric correction of satellite data and needs to be further explored (Hall et al., 2008, 2012; Koenig and Hall, 2010).

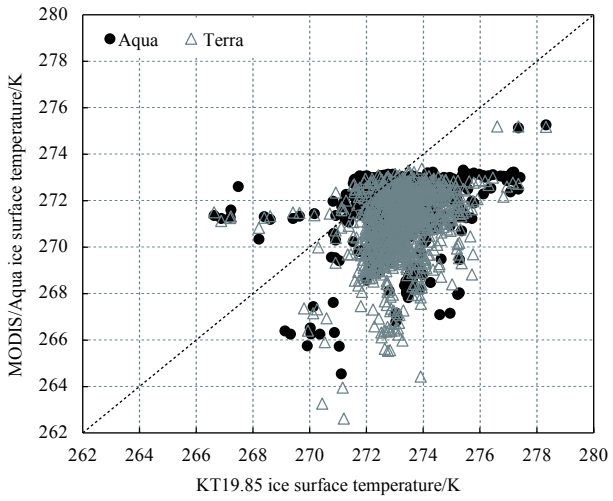

Fig. 4. Scatterplot of MODIS IST (Terra and Aqua) versus KT19.85 measurements for all six CHINARE cruises.

Table 2 presents the statistical results of the MODIS IST bias for each cruise. Similar with the results of all data, there is a close correspondence in temperature between the MODIS and KT19.85. The cold bias exists in both Aqua and Terra products. The Aqua MODIS IST bias is smaller than the Terra. The MODIS instruments onboard Terra and Aqua are effectively the same, except that on Aqua, Band 31 saturates at temperatures about 340 K while it saturates at around 400 K on Terra (Hall et al., 2008). The smaller dynamic range of the Aqua sensor in comparison with that of the Terra sensor provides a reasonable explanation for the smaller Aqua MODIS IST bias (Wenny et al., 2012).

As shown by the standard deviation and RMS error, the Aqua MODIS IST appears to have a better accuracy than Terra MODIS IST on some cruises, e.g., CHINARE-2008, CHINARE-2016. But the overall accuracy of the Aqua MODIS IST is comparable with

Table 2. Statistics of MODIS IST bias for each cruise

Cruise No.	Match points	Mean/K	Std dev/K	RMS/K
CHINARE-2008/Aqua	40	–2.0	1.8	3.3
CHINARE-2008/Terra	47	–2.7	2.3	5.7
CHINARE-2010/Aqua	113	–1.4	1.1	1.3
CHINARE-2010/Terra	144	–1.6	1.3	1.7
CHINARE-2012/Aqua	18	–2.7	1.6	2.7
CHINARE-2012/Terra	63	–2.0	1.6	2.3
CHINARE-2014/Aqua	324	–1.5	1.8	3.3
CHINARE-2014/Terra	389	–1.8	1.7	3.0
CHINARE-2016/Aqua	34	–2.9	1.3	1.8
CHINARE-2016/Terra	65	–3.5	1.7	2.9
CHINARE-2017/Aqua	5	–2.1	0.9	0.8
CHINARE-2017/Terra	265	–2.5	0.8	0.7

that of the Terra MODIS IST. Orbit characteristics of each satellite allow certain locations to be sampled only during a specific time on any given day. The MODIS instruments on the two satellites complement each other, providing information of more matching point between the satellite ISTs and in-situ measurements of different time and different locations in the Arctic Ocean.

5 Discussion

Thermal radiometers have been used previously for measuring surface temperature of snow and ice. A validation study of MODIS IST with KT19.85 measurements conducted during the Antarctic Remote Ice Sensing Experiment (ARISE) from September to October 2003 reported a variation of ±1.0 K (Scambos et al., 2006). Another validation study of AVHRR IST conducted during the SHEBA experiment in May 1998 reported a variation of ±1.5 K, in which the KT19.85 measurements are also used (Haggerty et al., 2003). Surface temperature range in this study (262–280 K) is more limited than that of previous studies, the overall standard deviation of MODIS IST bias (1.7 K for Aqua and 1.6 K for Terra) is comparable to previously reported values. In general, the IST difference between the satellite and *in situ* data is complicated by a variety of factors, including incorrectly assumed atmospheric conditions, undetected clouds in the satellite data, spatial and temporal variability in the surface temperature field, and errors of surface and satellite measurements (Key et al., 1994).

Satellite and *in situ* observations are not made at exactly the same time and location. Satellite data inevitably represent spatially averaged values. For the comparison of MODIS and KT19.85 ISTs in this study, though the KT19.85 measurements that fall within a grid cell of the MODIS data have been averaged, but the number of measurements that could be averaged varied from several to several hundreds and were very limited. Comparison of satellite data with surface point observations with 4 km× 4 km average may cause errors especially when ice and open water co-exist in the same grid box or during period of rapid meteorological changes (fronts, clear to cloudy etc.). During melting season, spatial variations of surface temperature are significant because of exposure of open water in leads, melt ponds and varying sea ice thickness. Melt ponds form when surface air temperature is persistently above freezing and they develop extensively. They can cover up to 50%–60% over the surface area of Arctic floes in summer (Eicken et al., 2004), and even rise up to 90% on a flat first-year ice and on ice in the early melt stage (Perovich et al., 2011). Surface temperature of leads is quite similar to that of the ponded ice.

To assess the possible errors arising from this spatial complexity, we first inspected the relationship of the MODIS IST bias with the corresponding sea ice concentration. Figure 5 shows that there is no obvious trend or a weak relationship, suggesting that most of the variability in MODIS IST bias is not a function of sea ice concentration. This is because surface temperatures are near freezing and relatively uniform during the melt season. The analysis of Haggerty et al. (2003) based on SHEBA data from late spring and summer also shows that surface temperature at a point approximates the mean surface temperature over the local area, with an RMS error of 0.75 K. That implies that the presence of mixed pixels will not increase the overall error in MODIS IST significantly.

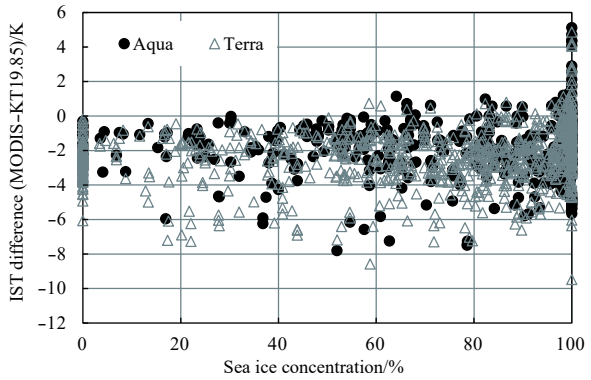

Fig. 5. Plot of the overall MODIS IST versus sea ice concentration.

It is interesting to note that the large positive biases were all found in mid-August 2014 north of the Chuckchi plateau, where the sea ice concentration was around 100% and ice thicknesses were large (Pan, 2015). Although it was close to the end of summer melt season in mid-August, ASPeCt sea ice observations conducted during CHINARE-2014 showed that the melt pond fraction can be up to 20%–30% in this area (Fig. 6). The lead/melt pond was much warmer than the surrounding ice throughout the summer melt season due to the radiative absorption by the open water in conjunction with weak vertical mixing that limits distribution of the absorbed energy (Haggerty et al., 2003). The relative high melt pond coverage in this area eventually leads to an increase in the spatial mean MODIS ISTs, and may be one explanation for the observed large positive biases here.

Among the variety of factors, undetected cloud may be an important source of errors in MODIS IST. In summer Arctic, there is more water vapor in the atmosphere, the cloud fractions are much higher than those in other seasons. Analysis of the time series of seasonally averaged cloud fraction over the Arctic ocean based on data from the AVHRR Polar Pathfinder (APP-x) and TIROS Operational Vertical Sounder (TPP) shows that mean summer cloud fraction for 1980–2001 was around 80%, and there is an increase with 1.5% per decade in cloud amount over the Arctic Ocean north of 60°N (Schweiger, 2004). Though we used satellite-derived IST points that were not cloud contaminated (clear-sky), undetected thin clouds and a varying atmospheric water vapor column may also influence the accuracy of satellite IST retrievals. To investigate the effect of cloud cover on MODIS ISTs, the relationship between the MODIS IST bias and cloud fraction was inspected. From Fig. 7, we found a slightly decreasing trend, which indicates that larger MODIS IST biases occur

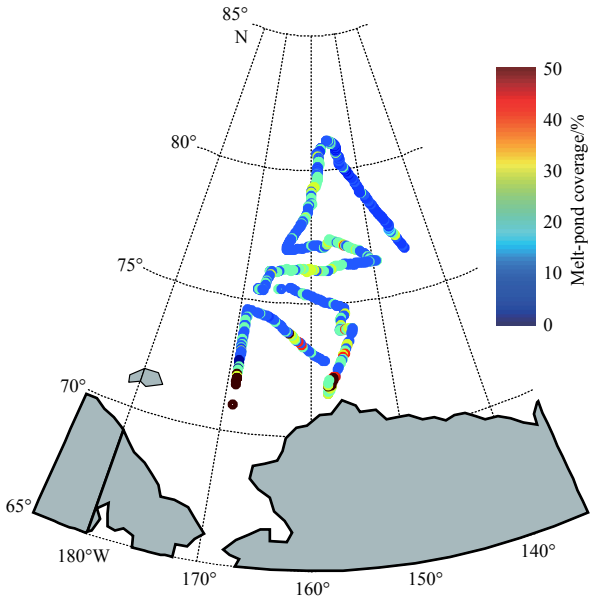

Fig. 6. Variations in melt-pond coverage over sea ice along the track of CHINARE-2014.

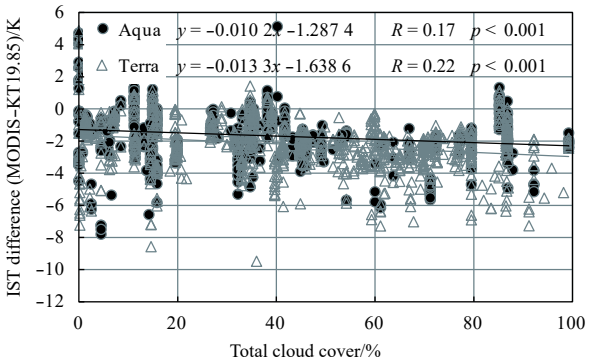

Fig. 7. Plot of the overall MODIS IST bias versus total cloud cover.

when cloud cover increases. In our study, clear-sky condition was determined from MOD/MYD35, the MODIS cloud-mask standard product. To ensure the amount of the data available, a pixel is considered clear if the cloud mask indicates a probability of 66% or more of clear skies for MOD/MYD29 series of IST products (Hall et al., 2015). Thus about half of the large MODIS IST cold biases (<–5 K) were found when the cloud cover is greater than the threshold value of 66%.

Though the standard MODIS cloud mask provides a conservative estimate of cloud over, it is virtually impossible to determine whether conditions are completely cloud free during automated algorithmic derivation of ISTs. The algorithm can fail to detect clouds or detect clouds falsely, especially for very thin stratiform cloud features, such as diamond dust, low ice-crystal haze, low thin stratus or cirrus without a spatial structure, and very thin fog. As shown in Fig. 7, a considerable number (30%–40%) of large cold biases (<–5 K) were found when the cloud cover is below 20%. Deep inspection of the results showed that the large cold bigases occurred north of 74°N during CHINARE cruises of 2008, 2010, 2012 and 2014, with the surface temperature in the floating ice area 3–5 K warmer than the air temperature there. The ASPeCt meteorological observations revealed that

sea fog was present for all these cases. Xie et al. (2001) presented that with the retreat of sea ice and exposure of open water, sea fog has been occurring more frequently in the Arctic in the summer in recent years and vapor fog is the dominant fog from in the Arctic floating ice north of 73°N. Taking one case during CHINARE-2012 (Fig. 8), there was just a cold front destroyed at the location of 83.44°N, 162.06°E on September 2, 2012, with the weak northerly wind (about 2 m/s) which keeps the inversion layer clear and windless. Similar meteorological pattern was found for all other cases. The agreement of the necessary conditions for the creation of vapor fog (Xie et al., 2001) can only account for the large cold biases that occur when the cloud cover is below 20%. Lack of independent cloud information precludes the possibility to derive a reasonable estimate for this error now. An additional cloud-clearing algorithm that uses texture and time-variance might be useful for fog detection and improving the MODIS IST retrievals (Hall et al., 2004).

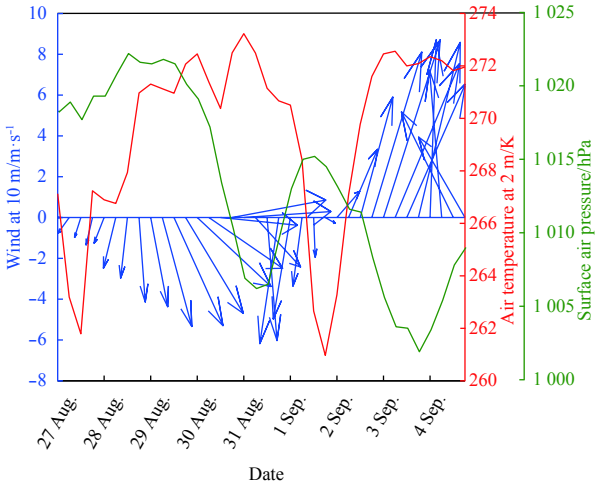

Fig. 8. Variability of wind at 10 m (blue), air temperature at 2 m (red), surface air pressure (green) for the case of September 2, 2012.

The MODIS–KT19.85 IST difference can also be influenced by errors in satellite and *in situ* measurements. The sensor's-view zenith angle (SeZA) and the solar zenith angle (SoZA) are two important parameters during the retrieval of MODIS IST. The SeZA relative to a site is a function of satellite orbit and is independent of temperature throughout the year, so this factor may contribute scatter but not the overall cold bias. There appears to be more variability in MODIS IST biases at larger SoZAs (Shuman et al., 2014). Because the most favorable daily observations that are near nadir and near noon local time were selected to build the MOD29E1D/MYD29E1D IST products used in our study, and the calibration of MODIS Bands 31 and 32 is best for snow/ice around 0°C (Wenny et al., 2012), the errors from the satellite measurements have been limited to a low level within algorithms and sensor capabilities. For the errors of *in situ* measurements, the standard deviation of KT19.85 surface temperature obtained during stationary viewing of uniform ice was typically 0.02–0.03 K when averaged over 1-min intervals (Scambos et al., 2006). Therefore, sky correction is presumed to be the main source of error in KT19.85 measurements. Assuming sky brightness temperature of approximately 260–280 K in the summer Arctic, absence of emissivity correction causes KT19.85 skin temperature to be approximately 0.5 K below actual skin temperature.

6 Conclusions and future work

The KT19.85 thermal radiometer has provided highly accurate surface temperature measurements spanning the entire summer period during six CHINARE cruises in the Arctic Ocean. These surface measurements were compared with collocated and coincident MODIS ISTs, which have a spatial resolution of 4 km and were obtained under cloud-free conditions. The average accuracy is (–1.6±1.7) K for Aqua MODIS IST and (–2.2±1.6) K for Terra MODIS IST based on 534 samples from Aqua and 973 samples from Terra. These results compare favorably with published findings and provide more detailed comparisons over multiple summer seasons. Results from the different cruises are consistent with one other indicates that the MODIS IST products are useful as part of the climate data record.

Our analysis shows that the large MODIS IST biases are primarily caused by spatial inhomogeneity and undetected cloud. Increased coverage of leads/melt ponds in the central Arctic Ocean and increased occurrence of vapor fog in the summer Arctic provide reasonable explanations for the large positive biases observed when sea ice concentration is high and the large negative biases observed when the cloud fraction is low. While the MODIS IST biases assessed in this study are only applicable to the atmospheric and oceanic conditions encountered during the six cruises, these conditions may be considered as typical Arctic summer conditions. To determine the source and actual magnitude of error in MODIS IST, future work is needed to improve the cloud screen algorithms for low thin cloud features (fog), and to collect extensive surface temperature measurements during other seasons and under other typical conditions. It is important to minimize uncertainties that could introduce biases in the long-term climate data record and also in other studies.

Acknowledgements

We thank CHINARE for the implementation of the ship-borne ice/sea surface temperature observations. We also thank the support staff onboard R/V *Xuelong* for helping to collect the *in situ* data necessary for this study. MODIS IST data was obtained from the National Snow and Ice Data Center (NSIDC).

References

Comiso J C. 2010. Polar Oceans from Space. New York: Springer-Verlag, 495, doi: 10.1007/978-0-387-68300-3

Comiso J C. 2012. Large decadal decline of the Arctic multiyear ice cover. Journal of Climate, 25(4): 1176–1193, doi: 10.1175/JCLI-D-11-00113.1

Dozier J, Warren S G. 1982. Effect of viewing angle on the infrared brightness temperature of snow. Water Resource Research, 18(5): 1424–1434, doi: 10.1029/WR018i005p01424

Eicken H, Grenfell T C, Perovich D K, et al. 2004. Hydraulic controls of summer Arctic pack ice albedo. Journal of Geophysical Research: Oceans, 109(C8): C08007, doi: 10.1029/2003JC001989

Haggerty J A, Maslanik J A, Curry J A. 2003. Heterogeneity of sea ice surface temperature at SHEBA from aircraft measurements. Journal of Geophysical Research: Oceans, 108(C10): 8052, doi: 10.1029/2000JC000560

Hall D K, Box J E, Casey K A, et al. 2008. Comparison of satellite-derived and in-situ observations of ice and snow surface temperatures over Greenland. Remote Sensing of Environment, 112(10): 3739–3749, doi: 10.1016/j.rse.2008.05.007

Hall D K, Comiso J C, Digirolamo N E, et al. 2012. A satellite-derived climate-quality data record of the clear-sky surface temperature of the Greenland ice sheet. Journal of Climate, 25(14): 4785–4798, doi: 10.1175/JCLI-D-11-00365.1

Hall D K, Key J R, Casey K A, et al. 2004. Sea ice surface temperature

product from MODIS. IEEE Transactions on Geoscience and Remote Sensing, 42(5): 1076–1087, doi: 10.1109/TGRS.2004.825587

Hall D K, Nghiem S V, Rigor I G, et al. 2015. Uncertainties of temperature measurements on snow-covered land and sea ice from *in situ* and MODIS data during Bromex. Journal of Applied Meteorology and Climatology, 54(5): 966–978, doi: 10.1175/JAMC-D-14-0175.1

Kearns E J, Hanafin J A, Evans R H, et al. 2000. An independent assessment of Pathfinder AVHRR sea surface temperature accuracy using the Marine Atmosphere Emitted Radiance Interferometer (MAERI). Bulletin of the American Meteorological Society, 81(7): 1525–1536, doi: 10.1175/1520-0477(2000)081<1525:AIAOPA>2.3.CO;2

Key J R, Collins J B, Fowler C, et al. 1997. High-latitude surface temperature estimates from thermal satellite data. Remote Sensing of Environment, 61(2): 302–309, doi: 10.1016/S0034-4257(97)89497-7

Key J R, Maslanik J A, Papakyriakou T, et al. 1994. On the validation of satellite-derived sea ice surface temperature. Arctic, 47(3): 280–287, doi: 10.14430/arctic1298

Koenig L S, Hall D K. 2010. Comparison of satellite, thermochron and air temperatures at Summit, Greenland, during the winter of 2008/09. Journal of Glaciology, 56(198): 735–741, doi: 10.3189/002214310793146269

Laxon S W, Giles K A, Ridout A L, et al. 2013. CryoSat-2 estimates of Arctic sea ice thickness and volume. Geophysical Research Letters, 40(4): 732–737, doi: 10.1002/grl.50193

Lei Ruibo, Li Zhijun, Li Na, et al. 2012. Crucial physical characteristics of sea ice in the Arctic section of 143°–180°W during August and early September 2008. Acta Oceanologica Sinica, 31(4): 65–75, doi: 10.1007/s13131-012-0221-0

Lindsay R W, Rothrock D A. 1994. Arctic sea ice surface temperature from AVHRR. Journal of Climate, 7(1): 174–183, doi: 10.1175/1520-0442(1994)007<0174:ASISTF>2.0.CO;2

Markus T, Stroeve J C, Miller J. 2009. Recent changes in Arctic sea ice melt onset, freezeup, and melt season length. Journal of Geophysical Research: Oceans, 114(C12): C12024, doi: 10.1029/2009JC005436

Minnett P J. 2003. Radiometric measurements of air-sea and air-ice temperature differences in the Arctic. In: 2003 IEEE International Geoscience and Remote Sensing Symposium. Toulouse, France: IEEE, doi: 10.1109/IGARSS.2003.1293748

Pan Zengdi. 2015. The report of 2014 Chinese Arctic Research Expedition (in Chinese). Beijing: China Ocean Press, 96–100

Perovich D K, Jones K F, Light B, et al. 2011. Solar partitioning in a changing Arctic sea-ice cover. Annals of Glaciology, 52(57): 192–196, doi: 10.3189/172756411795931543

Radionov V F, Bryazgin N N, Alexandrov E I. 1997. The Snow Cover of the Arctic Basin. Seattle, WA: Applied Physics Laboratory, University of Washington

Riggs G A, Hall D K. 2015. MODIS sea ice products user guide to Collection 6, https://landweb.modaps.eosdis.nasa.gov/QA_WWW/forPage/user_guide/MODISC6SeaIceproductsUserguide.pdf [2015-3-17/2019-5-1].

Scambos T A, Haran T M, Massom R. 2006. Validation of AVHRR and MODIS ice surface temperature products using *in situ* radiometers. Annals of Glaciology, 44: 345–351, doi: 10.3189/172756406781811457

Schweiger A J. 2004. Changes in seasonal cloud cover over the Arctic seas from satellite and surface observations. Geophysical Research Letters, 31(12): L12207, doi: 10.1029/2004GL020067

Shuman C A, Hall D K, Digirolamo N E, et al. 2014. Comparison of near-surface air temperatures and MODIS ice-surface temperatures at summit, Greenland (2008-13). Journal of Applied Meteorology and Climatology, 53(9): 2171–2180, doi: 10.1175/JAMC-D-14-0023.1

Wenny B N, Xiong X, Madhavan S. 2012. Evaluation of Terra and Aqua MODIS thermal emissive band calibration consistency. In: Proceedings Volume 8533, Sensors, Systems, and Next-Generation Satellites XVI. Edinburgh, United Kingdom: SPIE, doi: 10.1117/12.974230

Worby A P, Geiger C, Paget M J, et al. 2008. Thickness distribution of Antarctic sea ice. Journal of Geophysical Research: Oceans, 113(C5): C05S92, doi: 10.1029/2007JC004254

Xia Wentao, Xie Hongjie, Ke Changqing. 2014. Assessing trend and variation of Arctic sea-ice extent during 1979-2012 from a latitude perspective of ice edge. Polar Research, 33(1): 21249, doi: 10.3402/polar.v33.21249

Xie Simei, Xue Zhenhe, Jiang Dezhong, et al. 2001. Summer Arctic sea fog. Acta Oceanologica Sinica, 20(2): 183–196

Yu Y, Rothrock D A, Lindsay R W. 1995. Accuracy of sea ice temperature derived from the advanced very high resolution radiometer. Journal of Geophysical Research: Oceans, 100(C3): 4525–4532, doi: 10.1029/94JC02244